

Unexpected pressure induced ductileness tuning in sulfur doped polycrystalline nickel metal

Cheng Guo, Yan Yang, Liuxi Tan, Jialin Lei, Shengmin Guo, Bin Chen, Jinyuan Yan, and Shizhong Yang

Citation: *AIP Advances* **8**, 025216 (2018); doi: 10.1063/1.5022267

View online: <https://doi.org/10.1063/1.5022267>

View Table of Contents: <http://aip.scitation.org/toc/adv/8/2>

Published by the [American Institute of Physics](#)

Articles you may be interested in

[Numerical simulations to model laser-driven coil-capacitor targets for generation of kilo-Tesla magnetic fields](#)
AIP Advances **8**, 025103 (2018); 10.1063/1.5019219

[Transient pulse analysis of ionized electronics exposed to \$\gamma\$ -radiation generated from a relativistic electron beam](#)
AIP Advances **8**, 025001 (2018); 10.1063/1.5018727

[Direct bandgap type-I GeSn/GeSn quantum well on a GeSn- and Ge- buffered Si substrate](#)
AIP Advances **8**, 025104 (2018); 10.1063/1.5020035

[Effects of nanoparticle types and size on boiling feat transfer performance under different pressures](#)
AIP Advances **8**, 025005 (2018); 10.1063/1.5010809

[Shock-induced compaction of nanoparticle layers into nanostructured coating](#)
Journal of Applied Physics **122**, 165901 (2017); 10.1063/1.4996846

[Universal aspects of sonolubrication in amorphous and crystalline materials](#)
Journal of Applied Physics **123**, 035301 (2018); 10.1063/1.5003884

HAVE YOU HEARD?

Employers hiring scientists and
engineers trust

PHYSICS TODAY | JOBS

www.physicstoday.org/jobs



Unexpected pressure induced ductileness tuning in sulfur doped polycrystalline nickel metal

HPSTAR
518-2018

Cheng Guo,¹ Yan Yang,¹ Liuxi Tan,¹ Jialin Lei,² Shengmin Guo,³ Bin Chen,⁴ Jinyuan Yan,⁵ and Shizhong Yang^{1,3,a}

¹Department of Computer Science, Southern University and A&M College, Baton Rouge, LA 70813, USA

²Chemistry Department, University of California, Los Angeles, CA 90095, USA

³Department of Mechanical and Industrial Engineering, Louisiana State University, Baton Rouge, LA 70803, USA

⁴Shanghai Laboratory of HPSTAR, Center for High Pressure Science and Technology Advanced Research, Pudong, Shanghai 201203, China

⁵Lawrence Berkeley National Laboratory, Berkeley, CA 94720, USA

(Received 12 January 2018; accepted 9 February 2018; published online 20 February 2018)

The sulfur induced embrittlement of polycrystalline nickel (Ni) metal has been a long-standing mystery. It is suggested that sulfur impurity makes ductile Ni metal brittle in many industry applications due to various mechanisms, such as impurity segregation and disorder-induced melting etc. Here we report an observation that the most ductile measurement occurs at a critical sulfur doping concentration, 14 at.% at pressure from 14 GPa up to 29 GPa through texture evolution analysis. The synchrotron-based high pressure texturing measurements using radial diamond anvil cell (rDAC) X-ray diffraction (XRD) techniques reveal that the activities of slip systems in the polycrystalline nickel metal are affected by sulfur impurities and external pressures, giving rise to the changes in the plastic deformation of the nickel metal. Dislocation dynamics (DD) simulation on dislocation density and velocity further confirms the pressure induced ductilization changes in S doped Ni metal. This observation and simulation suggests that the ductilization of the doped polycrystalline nickel metal can be optimized by engineering the sulfur concentration under pressure, shedding a light on tuning the mechanical properties of this material for better high pressure applications. © 2018 Author(s). All article content, except where otherwise noted, is licensed under a Creative Commons Attribution (CC BY) license (<http://creativecommons.org/licenses/by/4.0/>). <https://doi.org/10.1063/1.5022267>

I. INTRODUCTION

The study of embrittlement, or ductility on the other end, of polycrystalline metals due to chemical impurities, such as sulfur (S), hydrogen (H), or phosphor (P) etc., is an important topic in material science, with a wide industrial applications. Since nickel (Ni)-based alloys have been broadly used, the Ni-S system has drawn great industrial attentions. Up to now, several mechanisms of Ni embrittlement, under different S concentrations, have been proposed. After extensive experimental work on S segregations, Heuer *et al.* proposed an embrittlement mechanism due to disorder-induced melting in Ni.¹ They also reported that a critical embrittlement S-concentration was found at 14.2 at.%. Later on, based upon first principles simulations, Yamaguchi *et al.* suggested that the dense sulfur segregation at the grain boundary (GB) regions could lead to a large GB expansion and result in the decrease of tensile strength of Ni by one order of magnitude.² However, early simulation work by Wu *et al.* showed the differences between the segregation energy of phosphorus in the GB regions and on the free surfaces, thus the mechanism of impurity induced embrittlement in bulk iron metal

^aCorresponding author: shizhong_yang@subr.edu

was proposed.³ More recently, Schusteritsch suggested that the presence of S impurities could cause substantial decrease of ductility in the GB regions, as a result of the competition between the grain decohesion and shear-induced plastic deformation due to grain boundary sliding.⁴ Although S segregation in the GB regions can be one of the major reasons, and especially at very high temperature S dopant can be easily segregated from bulk Ni metal to the GB regions, for Ni metal embrittlement, it cannot explain the fact that high S-concentration Ni could actually be super-plastic.⁵ A more recent statistics based percolation theory and molecular dynamics simulations predicted a critical amorphization S concentration of 13.6% by Yuan *et al.*,⁶ but no micro-atomic level mechanism was given in that theoretical and simulation study. As we know that the ductility or embrittlement is caused by the overall effect of dislocations. Obviously, further study on the shear stressed S-doped Ni metal samples using recent developed dislocation related synchrotron rDAC texture techniques⁷⁻⁹ can elucidate more details on understanding the embrittlement mechanism of doped Ni metal. Thus, we performed in-situ synchrotron radiation texture based dislocation characterization to understand the pressure effects on S doped polycrystalline Ni metal's embrittlement changes and analyzed the underline mechanisms. The DD simulations based on plastic deformation of single crystal model were performed and the results were analyzed to explain the observed abnormal embrittlement changes of S doped Ni polycrystalline metal under high pressure.

II. EXPERIMENT AND SIMULATION METHODS

In our experiment, nickel powders were mixed with nickel sulfide powders in a cold ball milling process. The atomic ratios of S in the mixture are 7 at.%, 11 at.%, 14 at.%, and 20 at.%, respectively. Based on (Material Analysis Using Diffraction) MAUD¹⁰ data fitting analysis, the result average polycrystalline size is 20 ± 5 nm. Synchrotron XRD data were collected on the NiS/Ni-S mixtures at Lawrence Berkeley National Laboratory (LBNL) BL-12-2-2 beamline to determine the possible phases formed under different pressures. Using a diamond anvil cell (DAC), radial compress-decompress experiments were performed (rDAC). The synchrotron XRD data was then collected at LBNL BL-12-2-2 to determine the possible formation of different phases, such as Ni₃S₂, NiS etc., in the Ni-S samples. The XRD data were also used for the texture and micro strain-stress analyses. Data collected from XRD measurement were analyzed using Fit2d¹¹ and MAUD software packages.

A series of first principle density functional theory based simulations for bulk Ni metal with various S substitution sites, concentration, and at different pressures were performed to obtain the shear moduli and Poisson's ratios which was used for dislocation dynamics (DD) simulation input parameters. Then, the effects of dislocation development were evaluated using the ParaDiS software package.¹² It is based on non-singular continuum theory of dislocations that allows accurate numerical calculations of dislocations in terms of multiple dislocation nodes.¹³ From our former research,^{7,9} the dislocation behaviors under pressure are similar for the Ni metals with particle size from 20 nm to 500 μm and bigger. Since ParaDiS based DD simulation is typically used for micro scale dislocation dynamics simulations, we set up isotropic models occupying $1 \times 1 \times 1 \mu\text{m}^3$ space and implemented face centered cubic (FCC) mobility law for static pressure simulation. Different Ni/S ratios were indirectly implemented by changing corresponding shear moduli and Poisson's ratios obtained from our first principle simulations mentioned above. The ductileness property can be analyzed by checking the changes of dislocation density and velocity.

III. RESULTS AND DISCUSSION

The MAUD software was employed to analyze the differential stresses and textures of the samples at each pressure. Inverse pole figure of compression direction (see Fig. 1) was used to represent the textures. These show the probability of finding the poles to lattice planes in the compression direction. The texture in 7 at.% S doped sample (shown at the top three graphs of Fig. 1) evolves at pressure as low as 0.5 GPa. At 13.5 GPa, an obvious development of texture strength can be found, with 1.12 multiples of random distribution (MRD). The texture strength keeps increasing when the pressure goes higher. The strongest texture strength can be observed when the pressure increased to

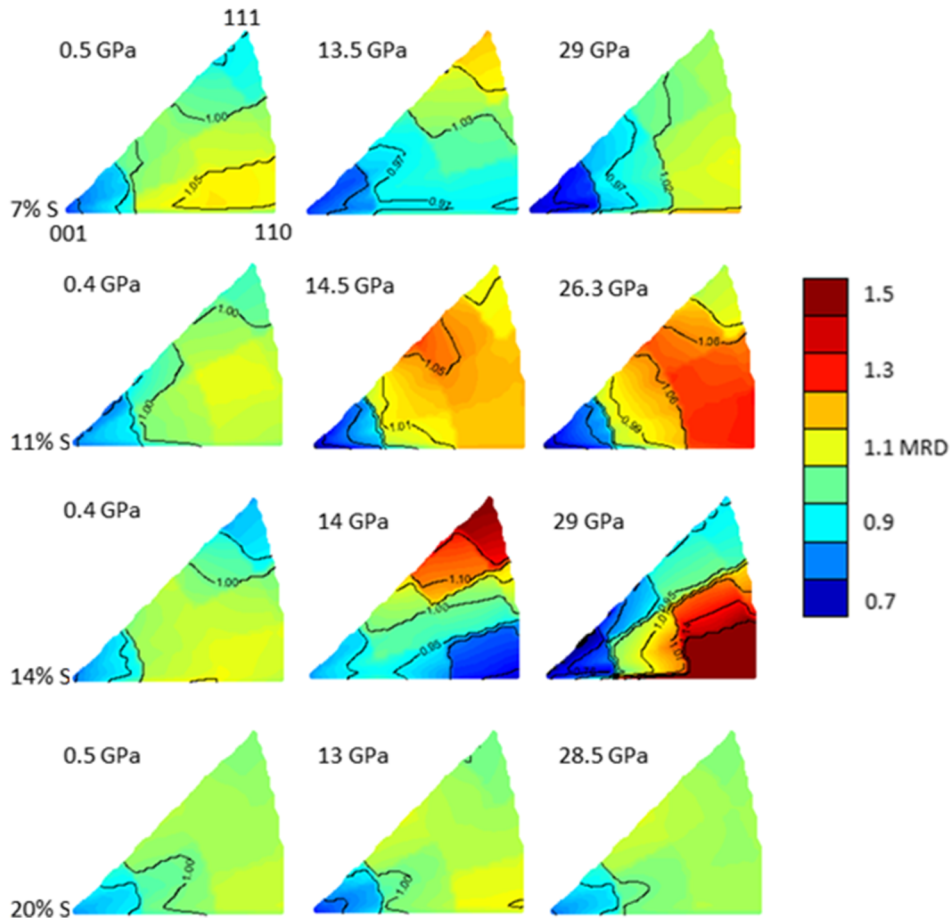


FIG. 1. Inverse pole figures of S doped nickel samples with 7 at.% (the top three graphs), 11 at.% (the three graphs in the second row), 14 at.% (the three graphs in the third row), and 20 at.% (the bottom three graphs) S concentrations along the normal direction (ND) under compression shear stress. Equal area projection and a linear scale are used. Texture strength is expressed as multiples of a random distribution (MRD), where MRD = 0 denotes random distribution, and a higher MRD number represents stronger texture and more ordered crystal orientational distribution.

29 GPa (1.14 MRD). The 11 at.% S doped sample (the three graphs in the second row) shared the similar trend of the 7 at.% sample, and presented the strongest texture at 26.3 GPa (1.48 MRD). The 14 at.% S sample (the three graphs in the third row) demonstrated the strongest texture among all samples at the intermediate pressure (14 GPa) and high pressure (29 GPa), with the texture strength of 1.22 MRD and 1.54 MRD, respectively. The texture observations indicate that dislocation-mediated plastic deformation is active for samples under high pressures. The texture diagrams also show the grain rotation due to the grain boundary sliding, which randomizes the grain orientation distribution. An abrupt texture strength increase is observed in the 14 at.% S doped sample when compared to that of the 11 at.% sample. The 20 at.% sample, however, does not have texture in (111) direction and no much difference exists when subject to different pressures, and showed weak texture strength, i.e. more brittle. The texture strength comparisons of Ni metal in the Ni-S samples indicated a critical dopant concentration of 14 at.% S dopant. For the cases of concentration lower than 14 at.%, the Ni-S samples always have dislocation-mediated plastic deformation; and the texture strength increases with pressure; In contrast, for a case of concentration exceeds 14 at.%, 20 at.% case, the Ni-S sample becomes more brittle and the texture pattern and intensity are very close. As showed in Fig. 2, the inverse pole figures for samples during decompression are highly consistent with those under medium pressure (12-14 GPa). Meanwhile, we noticed the relative strong textures at low pressure than original starting ones which indicates the existence of residual stress in the samples after decompression to

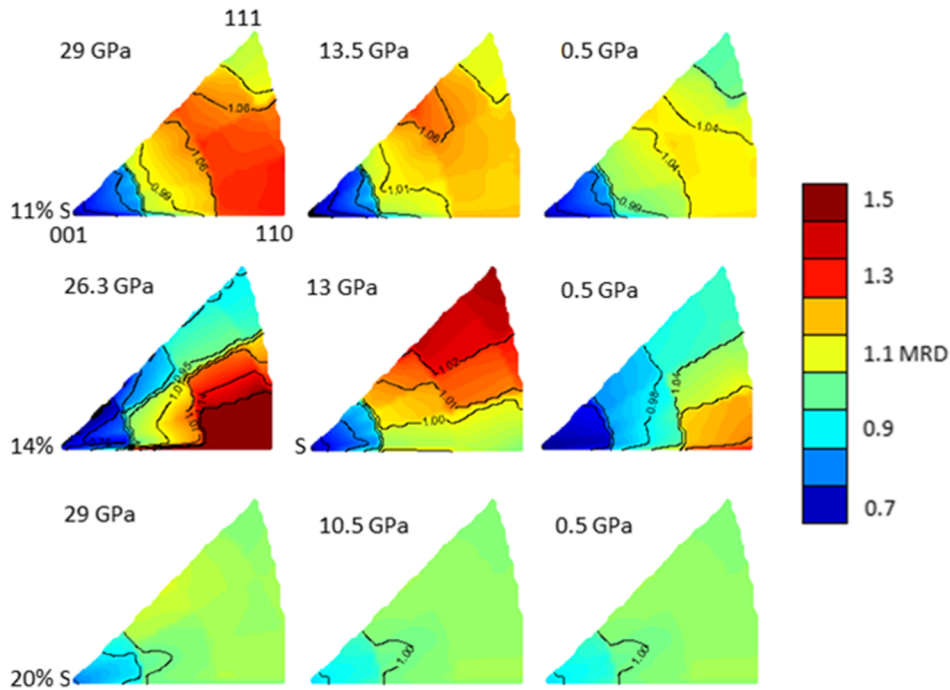


FIG. 2. Inverse pole figures of S doped nickel metal samples with 11 at.%, 14 at.%, and 20 at.% S concentrations along ND under decompression shear stress.

low pressure. Through the compression and decompression, the texture patterns of 20 at.% S dopant sample (shown at the bottom three graphs of Fig. 1) do not change much and keep very similar weak intensity at each orientation.

In order to gain a better understanding of the plastic deformation in the Ni-S samples, the X-Ray peak broadening of the samples under different pressures was analyzed, in the form of full width at half maximum (FWHM). The broadening is affected by three major factors: instrumental broadening, grain size effects, and stress-induced broadening. To characterize the instrumental broadening, LaB_6 is implemented in the test as the calibrant. Since we employed the same XRD facility, the instrumental broadening, which primarily depends on the equipment, are the same.⁷ From our recent experiment involves similar samples of polycrystalline nickel, the grain sizes are considered comparable. Thus the difference of broadening among different samples can only be attributed to the stress change.

The evolution of peak broadening of the four stressed samples shows substantial differences (Fig. 3). The broadenings of the three peaks have similar pressure dependencies, whereas the broadening evolution trend regarding pressure of 7 at.% and 11 at.% samples are quite different from that of 14 at.% and 20 at.% samples. Strain profiles in compression can affect peak broadening. For the 14 at.% and 20 at.% sample, the peak broadening trends showed that the strain and stress develops with pressure; when pressure reaches ~ 22.0 GPa, the strain and stress are reduced. The strain and stress change indicate that for samples with higher S concentrations, elastic deformation will occur, followed by fast reduction, especially for 20 at.% sample. The 14 at.% sample has less peak broadening while samples were compressed, which is consistent with the less brittle texture showing in Figs. 1 & 2.

To verify the embrittlement reduction observed from experimental results, we carried out a series of simulations for bulk Ni sample with dopant S atoms at substitution sites at 0, 15, and 30 GPa. The simulation result partially explained the experimental data that ductility improves along with the increase of pressure, but it is insufficient to clarify why 14 at.% sample is the most ductile one. First, a series of first principle simulations for bulk Ni sample with various S substitution sites at 0, 15 and 30 GPa were carried out. We chose 1 S atom substitution at the center for 12.5 at.% S doped Ni sample, and 2 S atoms at the center and corner for 25 at.% S doped Ni sample. The simulation results

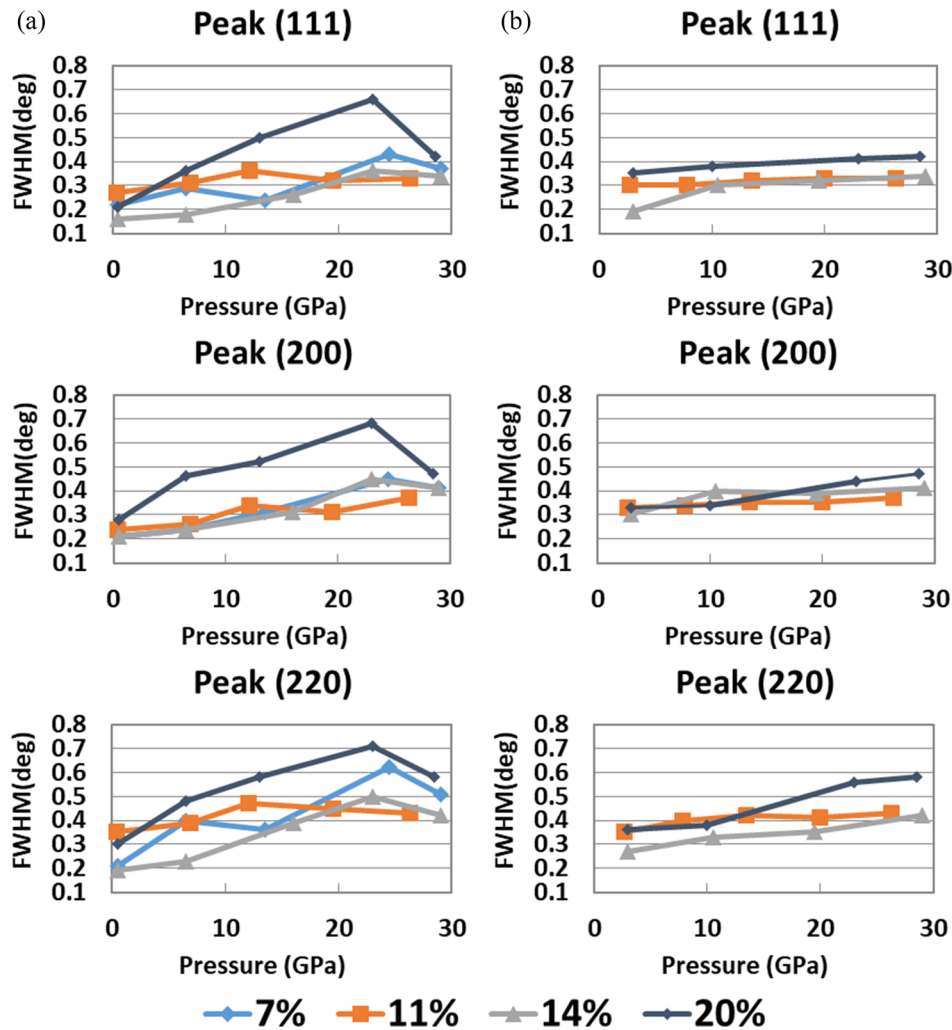


FIG. 3. The peak broadening of nickel in S doped Ni samples under compression and decompression shear stress. The full width at half maximum (FWHM) is used. The curves are offset for clarity. For the FWHM determination, the signal is integrated over 10 degrees around the compression direction. (a) represents the compression data, whereas (b) represents the decompression data.

of shear moduli and Poisson's ratios (Table I) will be used for ParaDiS input parameters discussed below.

The effects of dislocation development were evaluated using the ParaDiS software package. As showed in Fig. 4(b), the dislocation density results are consistent with our inverse pole figures, that 12.5 at.% S doped Ni metal has the highest dislocation density at high pressure, compared with other S concentrations. In terms of dislocation mobility, compared with pure Ni and Ni doped with 25 at.% S, the 12.5 at.% S doped Ni also revealed the highest dislocation velocity at high pressure (Fig. 4(c), 4(d), and 4(e)).

The broadening analysis of Ni in the Ni-S samples showed that the high S concentration samples, both 14 at.% and 20 at.%, from low pressure to ~ 22 GPa, exhibit mostly elastic deformation, then the broadening decreases afterwards. While for lower S concentration samples, the broadening development are substantially different. Since strain and stress change is the primary source of broadening, the ductility change in Ni-S samples can be deduced from dislocation movements and dislocation generation introduced by strain and stress change¹⁴ within the crystal structure of the Ni. On the other end, textural patterns at high pressures are similar among (20 nm – 500 nm) for FCC metals (Refs. 6 and 9), it is reasonable to use our ParaDiS simulation results at micron level to

TABLE I. Shear Moduli and Poisson's Ratios of Simulation Results.

Pressure	Model	Shear modulus (GPa)	Poisson's Ratio
0GPa	Pure	102.9	0.3226
	12.5%	75.24	0.3533
	25%	22.76	0.4486
15GPa	Pure	124.45	0.3331
	12.5%	94.36	0.3624
	25%	34.72	0.4427
30GPa	Pure	142.35	0.3404
	12.5%	112.6	0.3654
	25%	48.42	0.4350

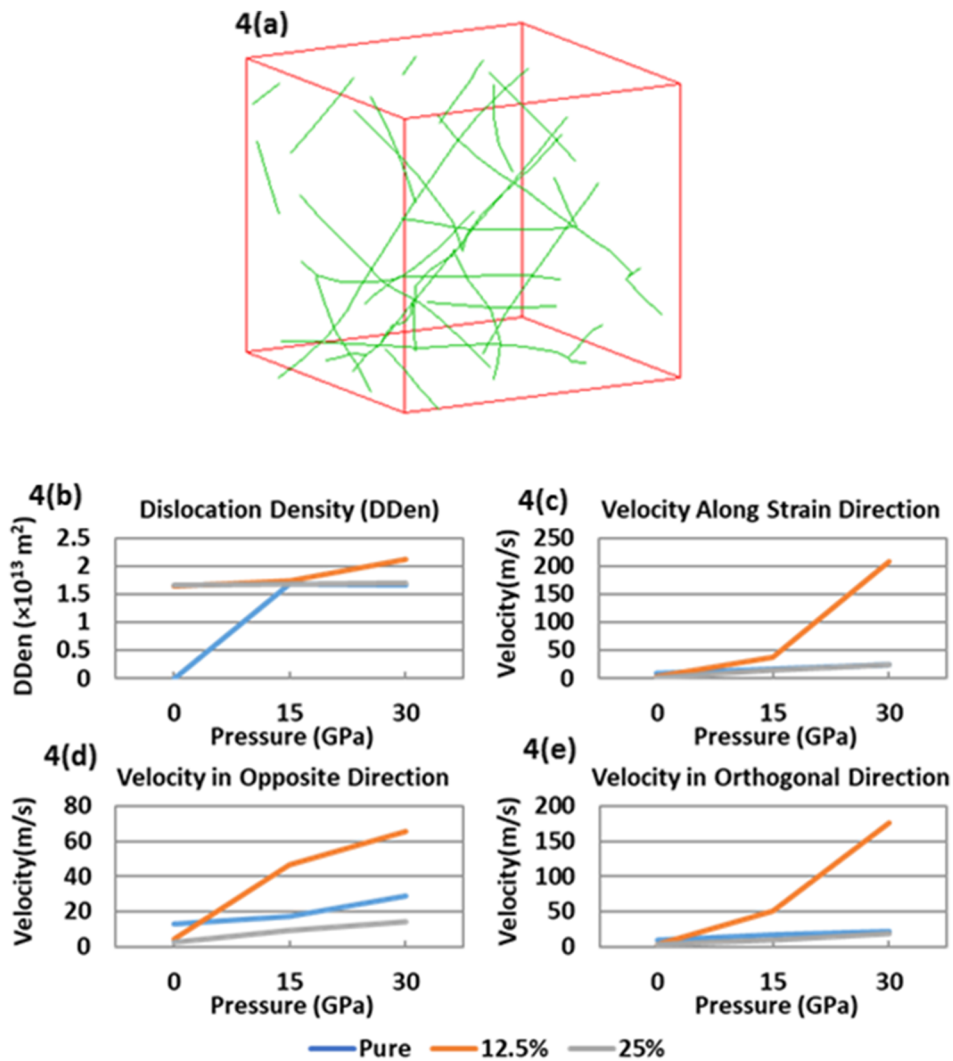


FIG. 4. (a) Initial dislocation setup for $1 \times 1 \times 1 \mu\text{m}^3$ cubic FCC Ni metal in ParaDiS. (b) Dislocation density of S doped Ni under different pressures in ParaDiS simulation. (c) The dislocation velocity component contributing to strain rate. (d) The dislocation velocity component in the opposite direction. (e) The dislocation velocity component in the orthogonal direction.

explain our samples at ~ 20 nm scale. At high pressure of ~ 30 GPa, the 12.5 at.% S doped Ni sample showed the highest dislocation densities and dislocation velocities along different directions, this is consistent with our earlier textural pattern, in which 14 at.% S doped sample showed the strongest

texture at high pressure of 26.3 GPa. According to Ashby,¹⁵ under compression, the plastic deformation induced increase in dislocation density, resulting in improvement of ductileness.

IV. CONCLUSION

In summary, we present a route for tuning Ni metal mechanical properties by adjusting the dopant concentration and external pressure. Our synchrotron XRD rDAC compress and decompress experiment observation of S doped Ni metal reveals that the 14 at.% S doped Ni metal is the most ductile one among all the cases studied under pressure at pressure from 14 GPa up to 29 GPa. The DD simulation confirms the pressure induced embrittlement changes. This discovery outlines a route of designing targeted metal ductileness by adjusting dopant concentration at high pressure.

ACKNOWLEDGMENTS

This research used beamline 12.2.2 of the Advanced Light Source, which is a DOE Office of Science User Facility under contract no. DE-AC02-05CH11231; was partially supported by NSF EPSCoR CIMM project under Award # OIA-1541079 and CIMM LINK project, NASA/LaSPACE LSU subcontract 77152 and 97732 (Primary Contract # NNX13AB14A), DOE Awards DE-FE0011550, and the Department of Computer Science. The computer simulation time is provided by LONI supercomputer allocations: loni_mat_bio6 ~ 10 (2015~2016) and LBNL NERSC Cori Phase I computer time. We thank Drs. Wei Cai and Amin Arbabian for their help in the ParaDis code running and for understanding of the simulation results and Prof. H. R. Wenk for data analysis discussion.

¹ J. K. Heuer, P. R. Okamoto, N. Q. Lam, and J. F. Stubbins, *J. Nuclear Materials* **301**, 129 (2002).

² M. Yamaguchi, M. Shiga, and H. Kaburaki, *Science* **307**, 393 (2005).

³ R. Wu, A. J. Freeman, and G. B. Olson, *Science* **265**, 376 (1994).

⁴ G. Schusteritsch and E. Kaxiras, *Modelling Simul. Mater. Sci. Eng.* **20**, 065007 (2012).

⁵ S. X. McFadden and A. K. Mukherjee, *Materials Science and Engineering A* **395**, 265 (2005).

⁶ Z. Yuan, H. P. Chen, W. Wang, K. Nomuna, R. K. Kalia, A. Nakano, and P. Vashishta, *J. Appl. Phys.* **110**, 063501 (2011).

⁷ B. Chen, S. V. Raju, J. Yan, W. Kanitpanyacharon, J. Lei, S. Yang, H. R. Wenk, H. K. Mao, and Q. C. Williams, *Science* **338**, 1448 (2012).

⁸ J. Lei, B. Chen, S. Guo, K. Wang, L. Tan, E. Khosravi, J. Yan, S. V. Raju, and S. Yang, *Appl. Phys. Lett.* **102**, 021901 (2013).

⁹ B. Chen, K. Lutker, J. Lei, J. Yan, S. Yang, and H. K. Mao, *PNAS* **111**, 3350 (2014).

¹⁰ <http://www.ing.unitn.it/~maud/>.

¹¹ <http://www.esrf.eu/computing/scientific/FIT2D/>.

¹² W. Cai, A. Arsenlis, C. R. Weinberger, and V. V. Bulatov, *J. Mech. Phys. Solids* **54**, 561 (2006).

¹³ V. Bulatov, W. Cai, J. Fier, M. Hiratani, G. Hommes, T. Pierce, M. Tang, M. Rhee, K. Yates, and T. Arsenlis, "Scalable line dynamics in ParaDiS," Proceedings of the 2004 ACM/IEEE conference on Supercomputing (2004).

¹⁴ C. Feltner and C. Laird, *Acta Metallurgica* **15**, 1633 (1967).

¹⁵ M. F. Ashby and J. D. Embury, *Scripta Metallurgica* **19**, 557 (1985).